MECHANO-THERMAL REDUCTION OF HEMATITE AND ANATASE MIXTURE BY TWO DIFFERENT FORMS OF CARBON AS REDUCTANT FOR IN-SITU PRODUCTION OF Fe-TiC –NANO-CRYSTALLINE COMPOSITE

S. Niksirat, Sh. Raygan and S. Moradi Ghiassabadi

* *shraygan@ut.ac.ir*

Received: November 2014 **Accepted: April 2015**

School of Metallurgy and Materials Engineering, College of Engineering, University of Tehran, Tehran, Iran.

Abstract: *In this research, two different carbonaceous materials (Graphite:G and Petrocoke:P) were separately compared in terms of the carbothermic reduction of hematite and anatase in order to synthesize Fe-TiC nano-crystalline composite by mechanically activated sintering method. Powders were activated in a planetary high-energy ball mill under argon atmosphere for 0, 2, 5, 10,and 20 h. Then, the activated powders were analyzed by XRD and SEM to investigate phase constituents and microstructure of the mixtures. Results proved that $Fe_2O_3$and TiO_2 were not reduced by carbonaceous materials even after 20h of milling. SEM investigations showed that G-mixture was more homogenous than P-mixture after 20h of milling, meaning that graphite-anatase-hematite was mixed satisfactorily. Thermogravimetry analysis was done on 0 and 20h milled powders. TG and DTG curves showed that mechanical activation led to almost 300°C decrease in the reduction temperature of hematite and anatase in both mixtures. In the next step, the powders were sintered in a tube furnace under argon atmosphere. In the G-mixture, anatase was reduced to titanium carbide at 1100°C; but, in the P-mixture, temperature of 1200°C was essential for completely reducing anatase to titanium carbide.Results of phase identification of the sintered powders showed that anano-crystalline iron-based composite with titanium carbide, as the reinforcement was successfully synthesized after 20 h high-energy milling of the initial powders and subsequent sintering occurred at 1200˚C for 1h.*

Keywords: *Mechanical Activation, Heat Treatment, Fe-TiC, Nano-crystalline Composite, Petrocoke, Graphite.*

1. INTRODUCTION

Examination of ferrous-based composite technology varies from inserts for machining tools to wear resistant plate for various applications [1].

Different oxide, nitride, and carbide particles can be used for reinforcing iron-based composites [2-6], among which TiC is more attractive because of having low density, high melting point, high hardness, corrosion resistant, and chemical stability with iron-based matrix[3-4, 7-12].

Thus far, different routes have been successfully utilized to synthesize Fe-TiC composites including casting [13-15], plasma smelting and spark plasma sintering [9, 11], self-propagating combustion synthesis [12, 16-18], powder metallurgy [2, 19], hot isostatic press [4], carbothermic reduction [20-21], and aluminothermic reduction [22]. In most of these methods, particle sizes are in the order of micron. Among the novel fabrication technology of nanoparticles in solid state, mechanical milling is one of the most common technologies [23]. Formation of nano-crystalline phases is an important characteristic of the microstructure produced by this process. Improved properties and performance are other advantages of this process over their conventional coarse-grained counterparts [24]. High-energy milling of reactants can excite processes, all of which influence heat treatment of powder[25]. The phenomenon of decrease in the onset temperature of a chemical reaction due to milling is known as mechanical activation [26]. High-energy mechanical milling is an effective process for synthesizing metal–ceramic composite powders, since it allows for the incorporation of the metal and ceramic phases into each powder particle [27]. Razavi et al.[7, 28] used this method to produce Fe-TiC nano-composite by ilmenite concentrate and black carbon.

Many researchers have focused on the reduction of hematite to iron [29-32] and reduction of titanium oxides to TiC [8, 33-34] by

[DOI: 10.22068/ijmse.12.2.56]

mechanically activated sintering method. Jing and Yisan[19] used carbon black with Ti and Fe powder to produce Fe-TiC composite. Das and Bandyopadhyay [35] believed carbon addition in various forms such as only graphite, graphite plus cast iron, and mostly cast iron plays an important role in the microstructure development of Fe–TiC composites synthesized by aluminothermic reduction of siliceous sand (a waste product of aluminum extraction plant containing oxides of Fe, Ti, Si, etc.) in the presence of carbon. Yang et al. [36] investigated the size effect of C particle on the porous formation of TiC particulate locally reinforced steel matrix composites. They found that, with the increased size of C particle, the porosities of the composites increased significantly. As sizes of C particle were lowered, hardness and wear resistance of the composites were increased[36].

In the present study, graphite and petrocoke were separately used to reduce hematite and anatase simultaneously in order to produce Fe-TiC nano-crystalline composite. The aim of this study was to investigate the effect of various forms of carbonaceous materials on production process and phase constituent of Fe-TiC nano-crystalline composite by an in-situ process using mechanical activation and subsequent heat treatment of Fe_2O_3-TiO_2-C powder mixture. The in-situ technique involves a chemical reaction which results in the formation of a very fine and stable ceramic phase within a metal matrix [19]. The advantages of the in-situ route are the clean surface of generated phase and homogenous distribution of the second phase in the matrix. In this situation, the matrix-reinforcement interface bonds tend to be stronger [19, 37-39].

The novelty of this process was in mechano-thermal reduction of iron and titanium oxides for the first time by two different forms of carbon, and the potential ability of two different forms of carbon to convert these raw materials directly into Fe and TiC and thus form a composite in a single step and impose better properties.

2. EXPERIMENTAL

In this study, graphite(>99% carbon, particle size 5-10μm), petrocoke(<120 μm), hematite powder(99% purity, <5μm), and anatase powder(99% purity,<5 μm) were used. The characteristics of petrocoke were examined by ASTM standard methods (D-3173, D-3174, and D-3175). The results are summarized in Table 1.

Graphite and petrocoke were separately used with 10wt% over stoichiometry to prevent the lack of carbon if unwanted oxidation happened during the milling. These raw materials were mixed according to reactions (1) and (2) in order to produce Fe-15wt%TiC nano-crystalline composite.

$$Fe_2O_3+3C=2Fe+3CO \quad (1)$$

$$TiO_2+3C=TiC+2CO \quad (2)$$

Planetary ball mill was used for the mechanical activation of raw materials.Ball-to-powder weight ratio (BPR) and rotational speed were 20:1 and 300 rpm in all the experiments, respectively. The milling process was carried out at room temperature using hardened steel vials (hardness of 60 HRC) and balls (hardness of 55 HRC), which were resistant to corrosion and wear. Three different ball sizes with the diameter of 5, 10, and 20 mm and equivalent weight were utilized. Different ball sizes were sometimes mixed to randomize the motion of the balls and increase the milling efficiency [40]. In order to

Table 1. Specifications of petrocoke used in this study

%Moisture	%Volatile Materials	%Ash	%Fixed Carbon
0	1.4	2.3	96.3

[DOI: 10.22068/ijmse.12.2.56]

protect the materials from oxidation, argon gas with the purity of 99.999% was charged in the vials.

At first, the mixtures of $Fe_2O_3/TiO_2/C$ (graphite or petrocoke) were activated for different hours (2, 5, 10, and 20 h).

After the milling, the powders were analyzed for morphological and structural characteristics. The powders were also investigated by X-ray diffraction (XRD) method (Philips Xpert pro diffractometer at 40kV and 100mA with $Cu_{k\alpha}$ radiation) and scanning electron microscopy (CamScan MV2300).

Mean crystallite size and the lattice microstrain of the milled particles were also analyzed at various stages of milling by XRD pattern analysis and Williamson–Hall method [41,42]:

$$\beta s_{ample}\cos\theta=K\lambda/d+2\ \varepsilon\ \sin\theta \quad (3)$$

where β_{sample} is full width at half-maximum (FWHM) of the milled powders, θ is position of peak maximum, K is Scherrer constant (about 0.9), λ is beam wave length, discrystallite size, and ε is lattice microstrain introduced by milling. For instrumental correction, Gaussian–Gaussian relationship was used [43]:

$$\beta"sample="\sqrt{(}\beta\_experimental\^2-\beta\_instrumental\^2) \quad (4)$$

where $\beta_{experimental}$ is measured FWHM and $\beta_{instrumental}$ is the FWHM of the annealed powders. Crystallite size of the heat treated powders was measured by Scherrer method after the instrumental corrections [41]:

$$\text{crystallite size}=k\lambda/B\cos\theta \quad (5)$$

0 and 20h activated powders were selected for simultaneous thermogravimetry analysis (NETZSCH STA 409 PC/PG) under flowing argon and heating rate of 10˚C/min from room temperature to1200˚C.

Thermodynamic information was calculated using HSC 4.0 software. At the next stage, the disk samples with the diameter of 12 mm and thickness of 4 mm were produced in a steel die using the load of 25kg/cm². Afterwards, heat treatment was performed in a tube furnace under argon atmosphere. The samples were held in the furnace at 1200°C for 1h and cooled down in the furnace to room temperature in argon atmosphere. In order to detect the type of the synthesized phases and components, XRD analysis was carried out.

3. RESULTS AND DISCUSSION

3.1. Phases and Morphology of the Powders

The XRD patterns of the un-milled (powder mixture prior to ball milling) and milled samples are shown in Figs. 1 and 2, respectively. All the raw materials were seen in the patterns of the un-milled sample. In the P-mixture, carbon peak was disappeared after 2h of milling because of the accumulation of energy and partial amorphization; but, in the G-mixture, disappearance occurred after 5 h. Reactivity and crystalline structure of the carbonaceous materials gradually changed during the course of milling; hence, the structure of petrocoke and graphite was transformed from crystalline into partially amorphous state. Thus, their peaks in the XRD patterns of the powder mixture were disappeared. Amorphization of carbonaceous materials during mechanical milling have been also reported by other researchers [31-35].

Petrocoke has lamellar and mosaic morphology, while morphology of graphite is flake-like [44 - 46]. Graphite is very soft and lubricant in nature. Petrocoke is not as soft as graphite and has no lubricant property, even it is brittle to some extent.It seems that breaking layers in petrocoke are easier than graphite and probably amorphisation in petrocoke occurs faster than graphite.

In both mixtures, maximum intense peak of anatase was not detected after 10 h of milling, while other peaks of anatase disappeared after 5 h of milling. This phenomenon occurred due to the energy storage in crystalline structure and partial amorphization of the anatase phase. Transformation of anatase into other phases such as rutile needed a great volume of energy that could not be produced even after 20 h of high-energy milling.

[DOI: 10.22068/ijmse.12.2.56]

Figs.1 and 2 also show broadening and decreasing intensity of the hematite peaks due to the mechanical deformation introduced into the powder, particle, and crystallite refinement and increasing lattice strain (ε). [35]. Accumulation of energy in the crystal structure led to high fraction of the boundary regions existing between nano-crystallites of hematite. These boundaries had a highly disordered structure which increased reactivity of the powder mixture.

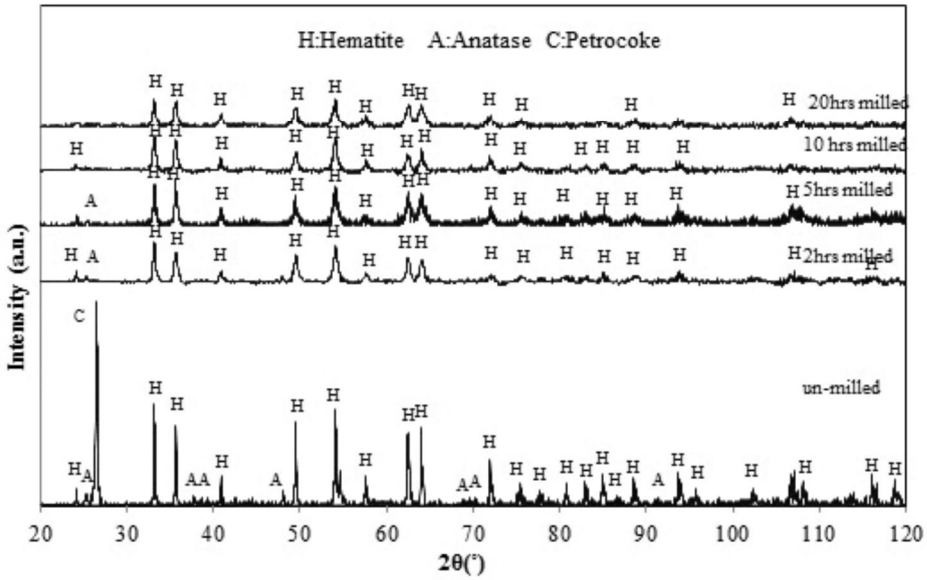

Fig.1. XRD patterns of the P-mixture after different milling times.

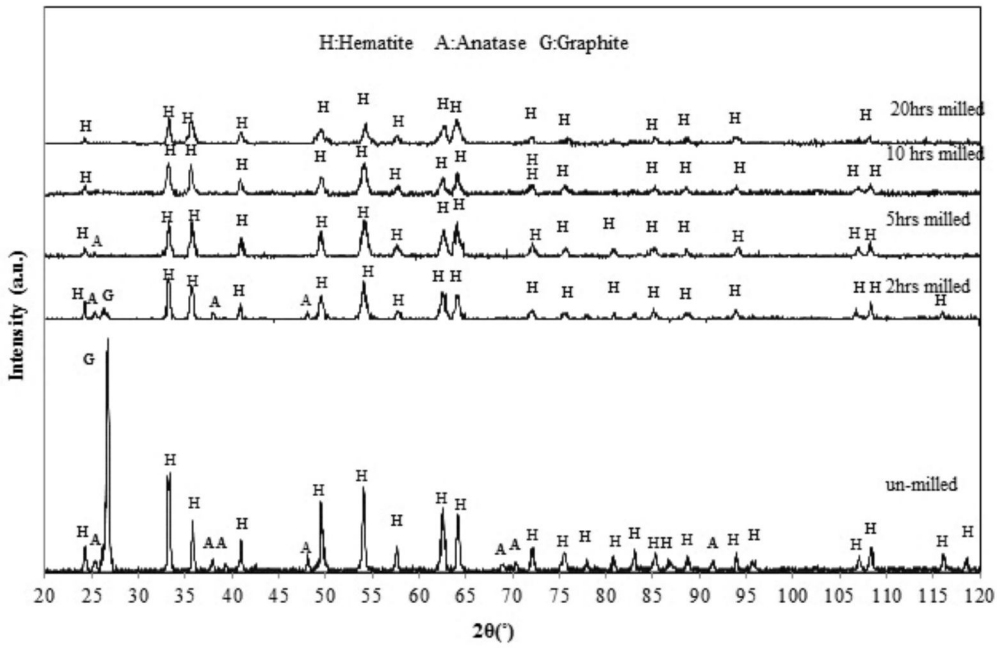

Fig. 2. XRD patterns of the G-mixture after different milling times.

[DOI: 10.22068/ijmse.12.2.56]

It can be concluded that anatase and hematite could not be reduced by graphite and petrocoke after 20 h of high-energy milling. In addition, new phases could not be observed in the XRD pattern of the milled powder, suggesting that no significant chemical reduction took place during the entire milling process.

The backscatter SEM images of the P- and G-mixtures are shown in Figs. 3 and 4, respectively. Fig.3.a and 5.a show the black flakes of petrocoke and graphite in the un-milled powder. White particles of hematite and grey particles of anatase in a spherical shape were obvious according to their atomic weight.

In the P-mixture, after 2 h of milling, (Fig.3.b), a non-homogenous structure was formed. In this figure, large agglomerates can be seen next to the individual particles. Increasing milling time to 10 h changed the size, shape, and number of the agglomerates. The number of the agglomerates was increased; but, their size was significantly decreased. It seems that the P-mixture, after 10 h of milling, greatly consisted of welded particles (Fig.3.c). It can be seen in Fig.3.d that, after 20 h of milling, a homogenous structure with a low number of small agglomerates was formed.

After 2 h of milling, the G-mixture had a more non-homogenous structure (Fig.4.b). There were more agglomerates than those in Fig.3.b. Fig.4.c shows the G-mixture after 10 h of milling. There were individual particles adjacent to some agglomerates. These agglomerates were very smaller than those in Fig.3.c. It can be observed that, after 20 h of milling, the G-mixture had a less number of agglomerates compared with Fig.4.c. It seems that the G-mixture was more

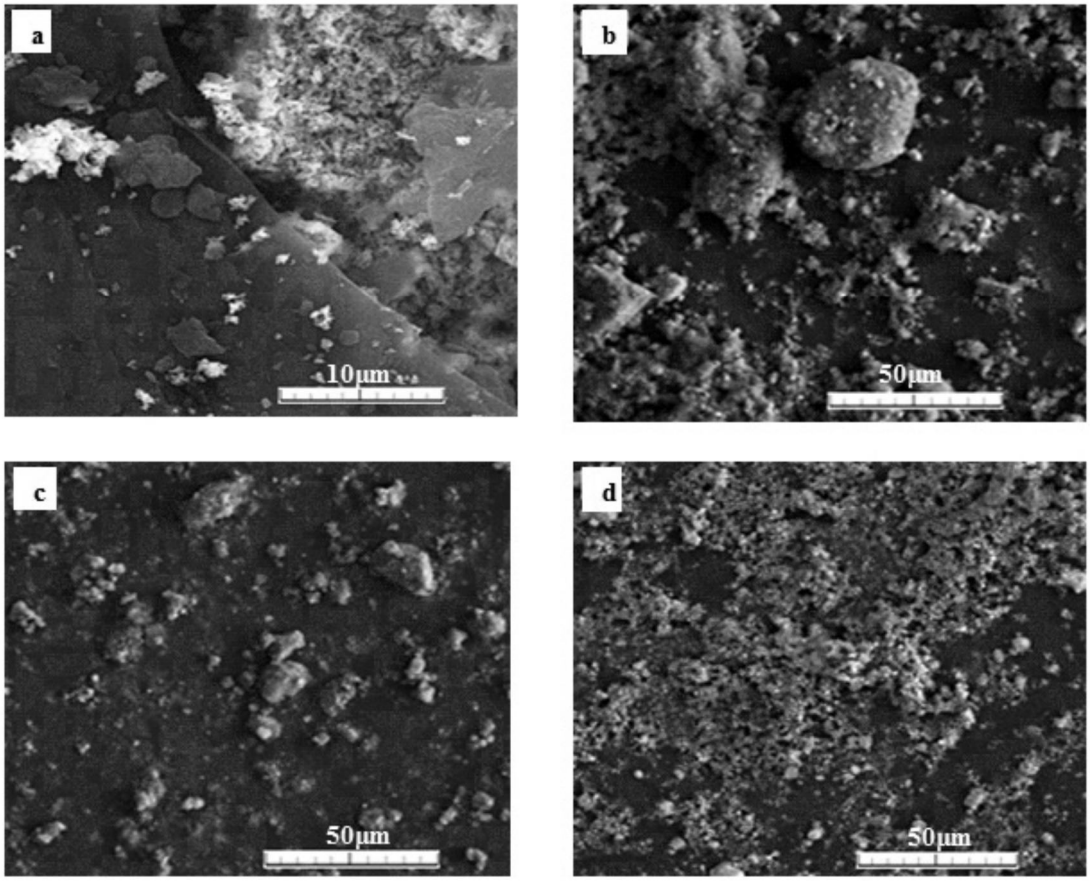

Fig. 3. Backscatter SEM images of P-mixture powder of a)un-milled, b)2h, c)10h, and d)20h milled mixtures.

[DOI: 10.22068/ijmse.12.2.56]

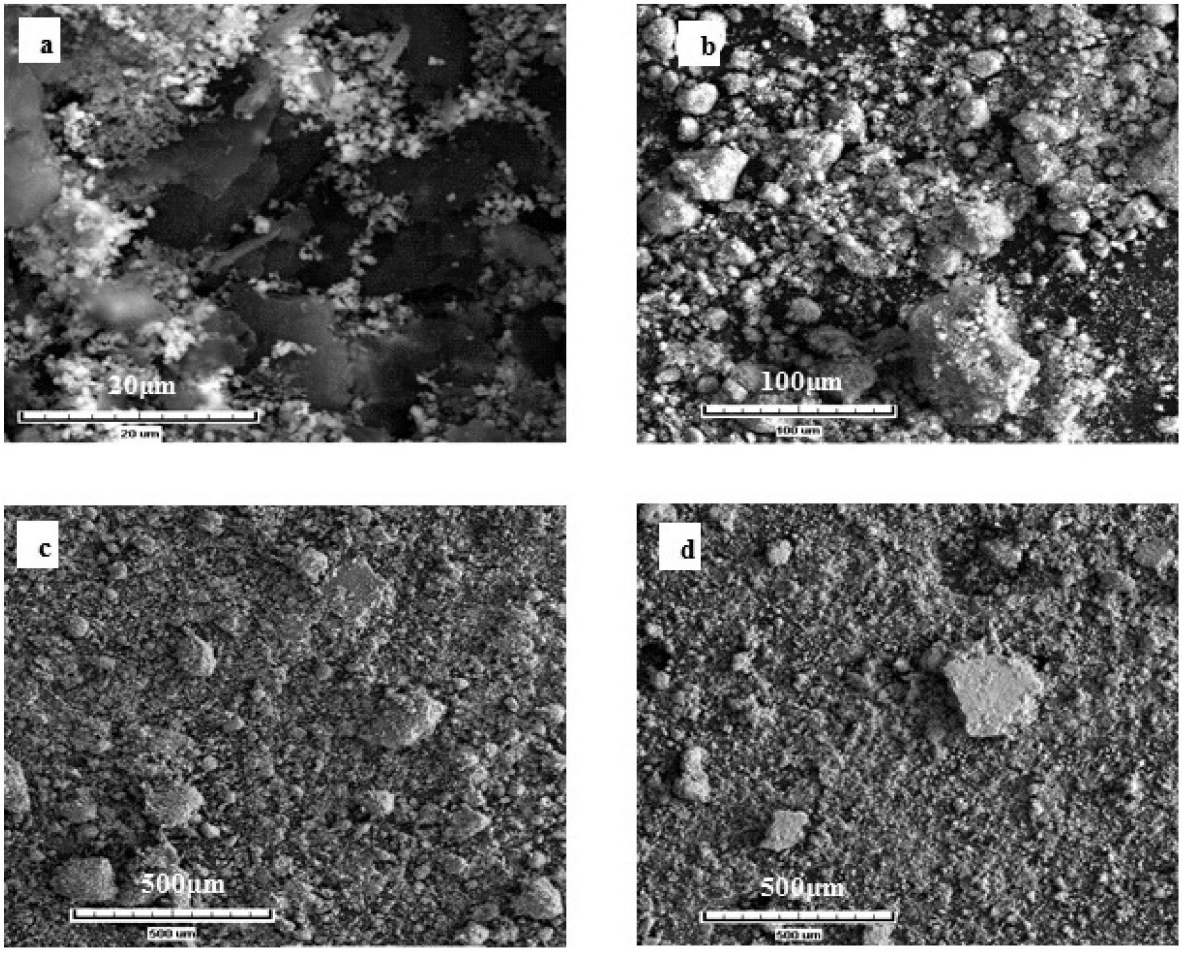

Fig.4. Backscatter SEM images of G-mixture powder of a)un-milled, b)2h, c)10h,and d)20h milled mixtures.

homogenous after 20h of milling: graphite-anatase-hematite was mixed satisfactorily.

There are two fundamental phenomena in mechanical milling: cold welding and fracturing. During the first hours of mechanical milling, like what was observed in this research, cold welding is usually predominant and a broad range of particle sizes is developed. With continued deformation, the particles get work hardened and fractured by a fatigue failure mechanism and/or the fragmentation of fragile flakes [26], which leads to a uniform structure.

3.2. Thermodynamics of Reduction

It has been reported that the reduction of Fe_2O_3 with C is not a simple reaction and goes through several stages [31, 33, 47, 48]. Fig.5 shows change of standard Gibbs free energy for reactions 6 to 11 in Gibbs free energy. These reactions are possible reactions that may happen during the carbothermic reduction of Fe_2O_3.

$$Fe_2O_3+3C=2Fe+3CO \quad (6)$$

$$3Fe_2O_3+C=2Fe_3O_4+CO \quad (7)$$

$$Fe_3O4+C=3FeO+CO \quad (8)$$

$$Fe_3O_4+4C=3Fe+4CO \quad (9)$$

$$FeO+C=Fe+CO \quad (10)$$

$$Fe_2O_3+C=2FeO+CO \quad (11)$$

[DOI: 10.22068/ijmse.12.2.56]

Based on this figure, direct reduction of hematite to iron (equation6) needs a great deal of energy. However, indirect reduction of hematite by the formation of other iron oxides with lower oxidation degree such as magnetite and wustite (Equations 7and 11) needs less energy; so, based on principle thermodynamics, at first, hematite is reduced to magnetite (Equation 7),instead of reduction to Fe or wustite (Equations 6 and 11). In the next step, magnetite can be reduced to iron directly or wustite in one step and then wustite can be reduced to iron. Based on Fig.5, direct reduction of magnetite to iron needs less energy than its reduction to wustite; so, the curves of ΔG-T dictates this trend: hematite→ magnetite →iron. More studies on hematite reduction under argon atmosphere have shown that this trend is not true in that condition because of some unknown kinetic parameters, and magnetite cannot be directly reduced to iron. Hematite under argon atmosphere is reduced to iron according to this trend: hematite → magnetite →wustite→iron (Equations 7, 8, and 10). This trend has been also confirmed by other researchers. [31, 33, 47, 48] .Kashiwaya et al. [47, 48] defined "nano-reactor" for understanding the high reduction rate. Preconditions of nano-reactor are:

1. Size of hematite should be less than 1mm.

2. The hematite particle should be surrounded by carbon or struck into carbon particle, which supports the contact between hematite and graphite particles and completion of the reaction [47, 48].

There is no report on the formation of Fe_3C at these stages. The results of this study also did not show any trace of iron carbide, which was in agreement with the above-mentioned mechanism.

It has been proved that reduction of titanium dioxide needs higher temperature than predicted thermodynamic temperatures and there are some suboxides that can be formed during TiO_2 carbothermic reduction. These suboxides can decrease energy barrier and essential

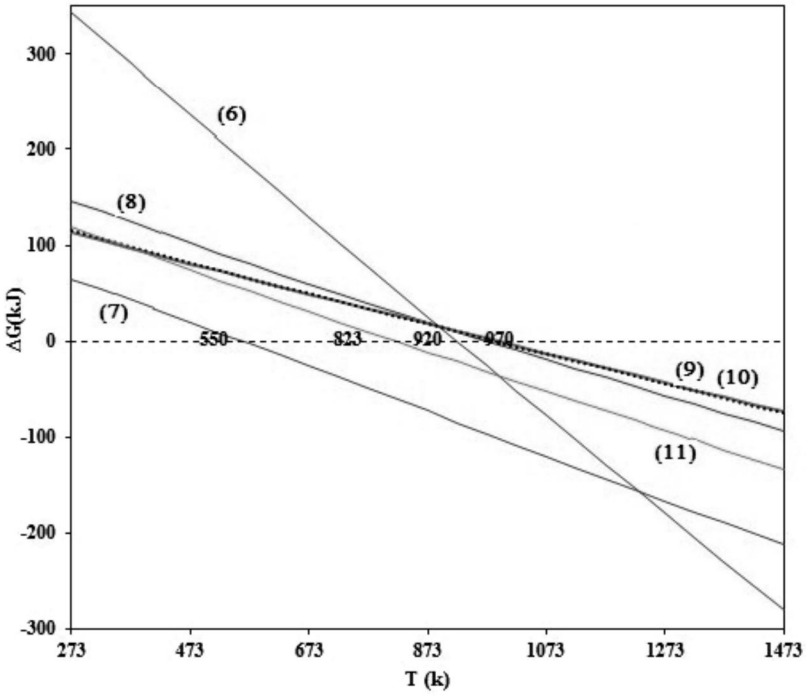

Fig.5. Change of standard Gibbs free energy for reactions 6 to 11.

[DOI: 10.22068/ijmse.12.2.56]

temperatures. Equations 12 to 26 are possible reactions during the carbothermic reduction of TiO_2. Swift and Koc [49] predicted the following trend for the carbothermic reduction of TiO_2:

$$TiO_2 \rightarrow Ti_4O_7 \rightarrow Ti_3O_5 \rightarrow TiC.$$

But Razavi et al.[34]suggested another trend:

$$TiO \rightarrow Ti_3O_5 \rightarrow Ti_2O_3 \rightarrow TiCxOy \rightarrow TiC.$$

Direct reduction of TiO_2 to TiC follows Equation 26. Standard change in Gibbs free energy of this reaction reaches zero at about 1300˚C; but, some kinetic parameters postpone this reaction until the temperatures of upper than 1700˚C; so, the formation of suboxides is expected.

The degree of the carbothermal reduction of the titanium dioxide mainly depends on the interface reaction between the titanium dioxide and carbon in their contact area. The degree of carbothermal reduction increases with decreasing particle size of the starting powders because of an increment in the contact area [50].

$$4TiO_2+C=Ti_4O_7+CO \quad (12)$$

$$3TiO_2+C=Ti_3O_5+CO \quad (13)$$

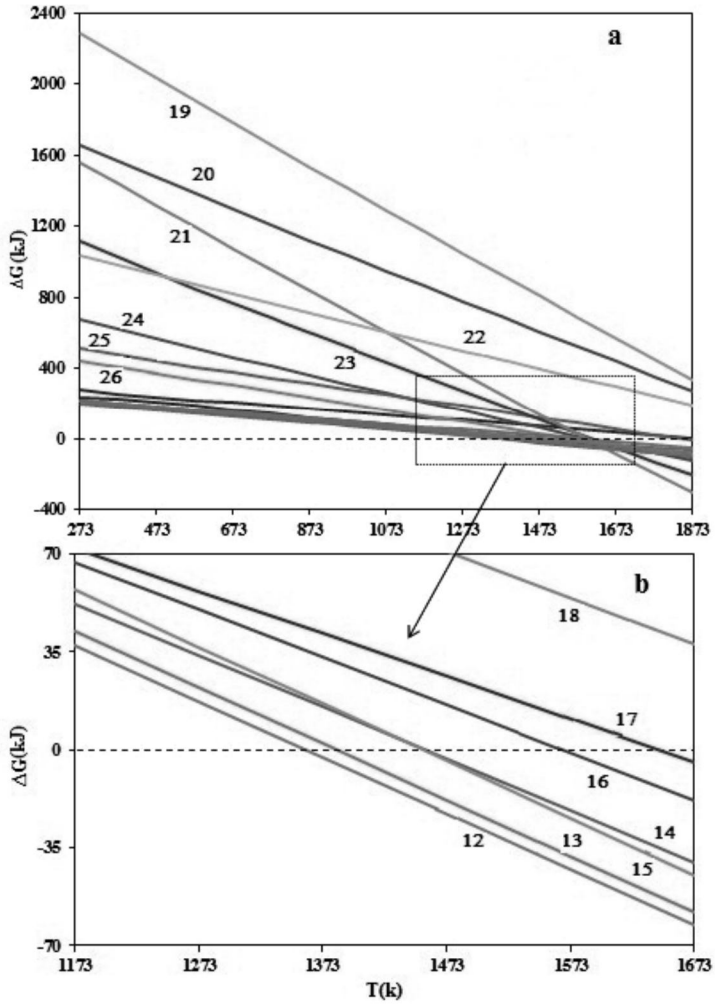

Fig. 6. Change of standard Gibbs free energy of reactions 12 to 26.

[DOI: 10.22068/ijmse.12.2.56]

$$2TiO_2+C=Ti_2O_3+C \quad (14)$$

$$3Ti_4O_7+C=4Ti_3O_5+CO \quad (15)$$

$$Ti_4O_7+C=2Ti_2O_3+CO \quad (16)$$

$$Ti_3O_5+C=3Ti_2O_3+CO \quad (17)$$

$$Ti_2O_3+C=2TiO+CO \quad (18)$$

$$Ti_4O_7+7C=4Ti+7CO \quad (19)$$

$$Ti_3O_5+5C=3Ti+5CO \quad (20)$$

$$Ti_4O_7+11C=4TiC+7CO \quad (21)$$

$$Ti_2O_3+3C=2Ti+3CO \quad (22)$$

$$Ti_3O_5+8C=3TiC+5CO \quad (23)$$

$$Ti_2O_3+5C=2TiC+3CO \quad (24)$$

$$Ti_3O_5+2C=3TiO+2CO \quad (25)$$

$$TiO_2+3C=TiC+CO \quad (26)$$

3.3. Thermal analysis

Thermogravimetry (TG) analysis was done on the un-milled and 20 h milled G-and P-mixture powders under Ar atmosphere. Fig.7.a and b shows TG and differential thermogravimetry (DTG) results, respectively. Increased reactivity from mechanical activation was confirmed by comparing the results of the TG tests of un-milled and 20 h milled powders. In Fig.7.a, the mass loss up to 800 and 780˚C for the un-milled G- and P-mixture powders (first mass loss), which was the onset of the first peak in DTG curves(Fig.7.b), was related to the adsorbed gases on the surface of the powder. During the mechanical activation, some gases and humidity can be adsorbed from the environment due to decreasing particle size. Consequently, slight weight loss could be observed at the initial stages of TG test.

The second mass loss in TG curve, which is notably steeper than the first one, was related to the reduction of iron oxide by carbonaceous materials. This reduction consisted of three separated reaction sin the un-milled powders, i.e. reduction of hematite to magnetite, magnetite to wustite, and wustite to iron. The starting point of these stages for the un-milled sample was 800˚C and 865 ˚C for the G- and P-mixtures, respectively, which decreased to 500 and 423°C for 20 h of milling in the G- and P-mixtures, respectively. It can be observed that reduction stages were overlapped in the milled mixture powders.

These substantial differences between the onset reduction temperature of the un-milled and milled powders can be related to the mechanical activation and presence of crystal defects such as dislocations, vacancies, stacking faults, and increased number of grain boundaries [24].

In the G-mixture, formation of iron was completed at 1090˚C for the un-milled sample and this temperature decreased to 785˚C for the 20h milled G-mixture. In the P-mixture, formation of iron was completed at 1190 and 800˚C for the un-milled and 20h milled powders, respectively. Hence, 20 h milling of both mixtures was adequate for complete reduction of hematite to iron at less than 1000°C.

According to the amount of weight loss of the powder calculated from TG curves, it seems that, in the un-milled powder mixture, there were no traces of reduction in anatase phase and the weight loss was attributed only to the hematite reduction.

Metallic oxides are categorized as brittle materials. Graphite is a lubricant material that can be categorized as a ductile material. In brittle-ductile systems, at the initial stages of milling, ductile particles (graphite) get fattened by the ball-powder-ball collisions, while brittle oxide particles get fragmented/comminuted. These fragmented brittle particles tend to become occluded by the ductile constituents and trapped in the ductile particles. The brittle constituent is closely spaced along the interlamellar spacing. With further milling, the ductile powder particles get work hardened and the lamellae gets convoluted and refined. The composition of the individual particles converges to the overall composition of the starting powder blend. With continued milling, the lamellae gets further refined, the interlamellar spacing is decreased, and the brittle particles get

[DOI: 10.22068/ijmse.12.2.56]

uniformly dispersed, if they are insoluble, in the ductile matrix [24, 51].

Despite graphite, petrocoke is a brittle carbon material. The brittle components get fragmented during milling and their particle size gets reduced continuously. However, at very small particle sizes, powder particles behave in a ductile fashion and further reduction in size is not possible; this is termed the limit of comminution. During the milling of brittle-brittle component systems, it has been observed that harder (more brittle), here iron oxide and titanium oxide,

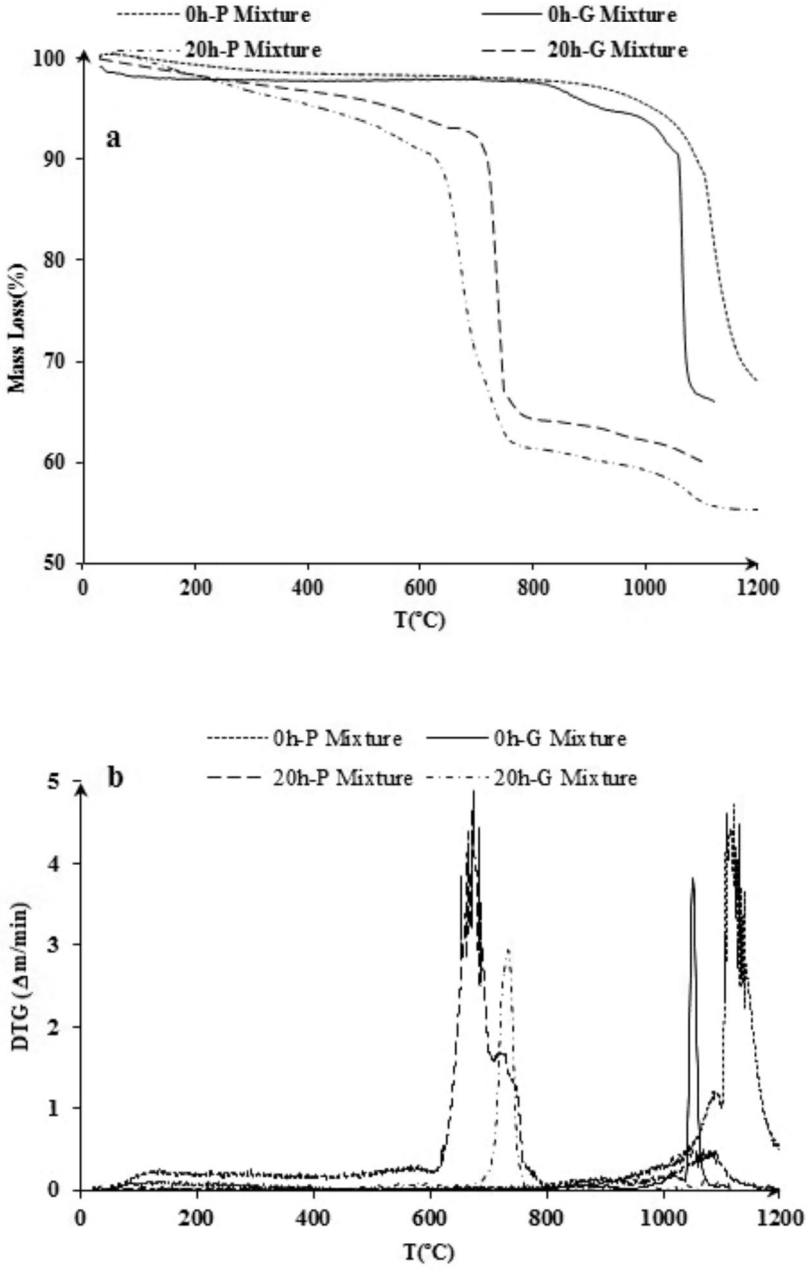

Fig.7. a) TG, b)DTG results of the P- and G-mixtures in different conditions.

[DOI: 10.22068/ijmse.12.2.56]

component gets fragmented and embedded in the softer (less brittle), here petrocoke, component. According to the results of TG tests, the P-mixture was activated more than the G-mixture. Also, in the P-mixture, the reactions took more time than the G-mixture, which can be due to different systems in mechanical activation and different structures of both carbonaceous materials.

The third mass reduction in the 20h milled powders was relevant to the transformation of anatase to titanium carbide. The first titanium suboxide in the reduction process of TiO_2 was Ti_4O_7. It seems that the formation of this phase started after the complete reduction of hematite to iron. This stage of reduction in the G- and P-mixture began at 785 and 800°C, respectively. Reduction stages of Ti_4O_7 to other titanium suboxides and then titanium carbide were nearly overlapped and it was not possible to determine the completion of every stage and starting of the next one. However, based on the mass loss in Fig.7.a, it can be concluded that the formation of TiC was completed at 1080 and 1200°C in the G- and P-mixture, respectively.

3.4. Heat Treatment of the Activated Powder

XRD patterns of the mechanically activated and sintered at1100 and 1200˚C mixtures are shown in Fig.8 .a-c. The results showed that, after the heat treatment of the un-milled G-mixture, hematite was reduced to iron; but, anatase was reduced to some titanium suboxides (Fig.8a).

XRD patterns of the 10h milled mixtures showed that hematite was completely reduced to iron. Fig 8.b shows that iron and titanium carbide were synthesized in the 10h milled G-mixture after heat treatment at 1200˚C.However, small peak of graphite can be seen in the figure. According to Fig.8c, after the heat treatment of 10h milled P-mixture at 1200˚C, iron and TiC phases were formed; but, there was one peak of Ti_2O_3 in the pattern which proved that, in the P-mixture, this condition was not suitable for completely reducing anatase to titanium carbide.

Fig.8.b and c shows that, in both mixtures, Fe-TiC composites were formed after 20h of milling

Table 2. Crystallite size of Fe and TiC in Fe-TiC nanocomposite after heat treatment at 1200°C

	Milling time(h)	Fe-Crystallite size(nm)	TiC-Crystallite size(nm)
Graphite	10	43	28
	20	51	30
Petrocoke	10	77	47
	20	68	39

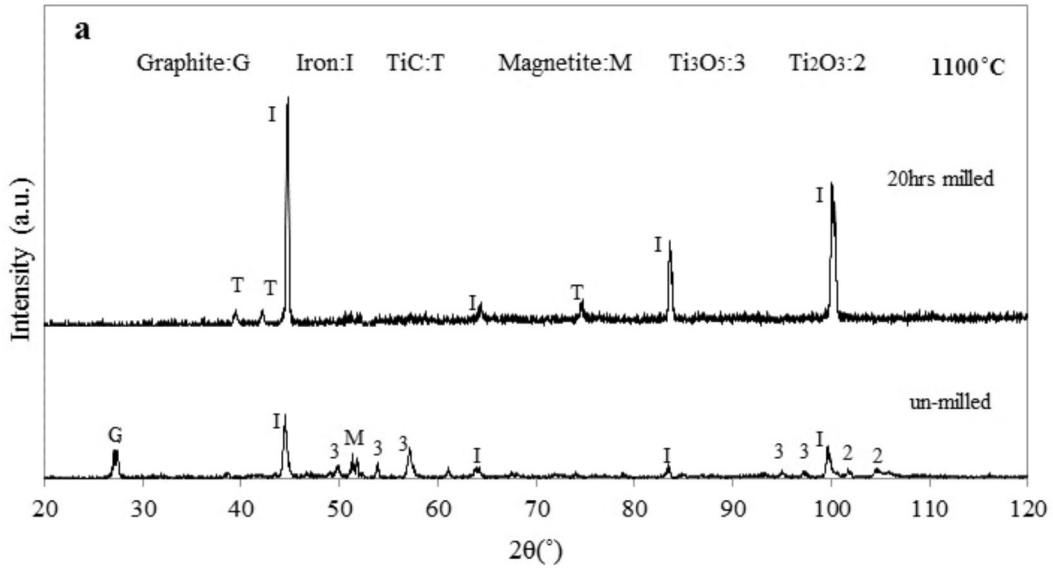

[DOI: 10.22068/ijmse.12.2.56]

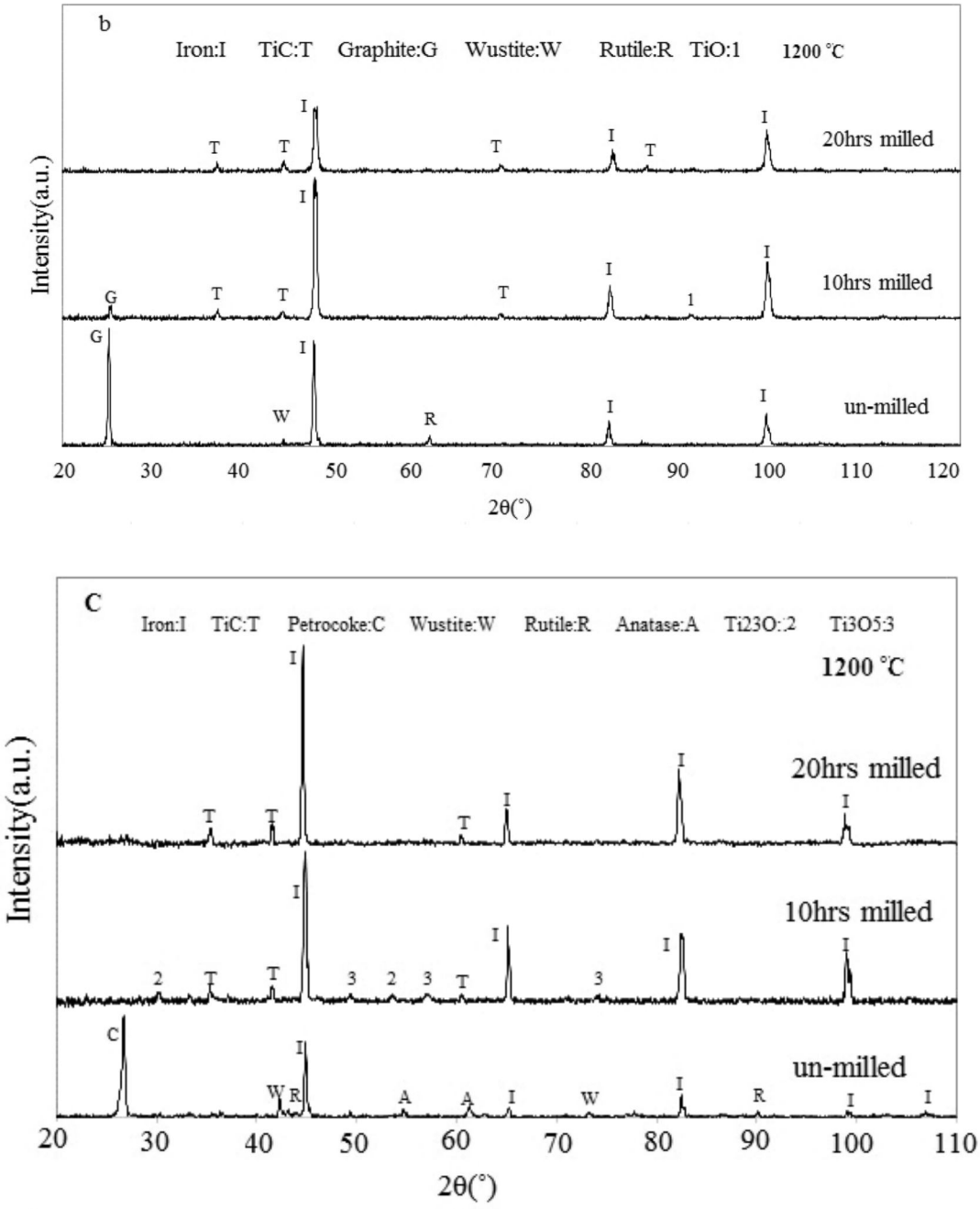

Fig. 8. XRD patterns of mechanically activated and sintered G-mixture at a) 1100°C, b)1200°C, and c) P-mixture at 1200°C.

and subsequent heat treatment at 1200˚C. Results of the measurements of Fe and TiC crystallite size by Scherrer formula are summarized in Table 2. It can be observed that the crystallite size in the P-mixture was higher than that in the G-mixture. Accordingly, Fe and TiC nano-crystalline composites were formed in both powders.

4. CONCLUSIONS

In this study, production of Fe-TiC nanocomposite by simultaneous carbothermic

[DOI: 10.22068/ijmse.12.2.56]

reduction of iron and titanium oxide was investigated. Using graphite(G-mixture) and petrocoke (P-mixture) as reductants was successful for synthesising Fe-TiC nanocrystalline composite by mechanically activated sintering method. From the obtained results, the following conclusion can be drawn:

1. Hematite and anatase mixture could not be reduced by petrocoke or graphite even after 20 h of high energy milling.
2. Mechanical activation led to almost 300°C decrease in the reduction temperature of hematite and anatase.
3. In the un-milled G- and P-mixture after heat treatment at 1100°C, only hematite can be reduced to iron and there was no symptom of TiO_2 reduction.
4. In the G-mixture, anatase was reduced to titanium carbide at 1100°C,; but, in the P-mixture, 1200°C was essential to completely reduce anatase to titanium carbide.
5. Fe-TiC nano-crystalline composite was synthesized in the 20h milled P- and G-mixtures after heat treatment at 1200˚C.

REFERENCES

1. Hathaway, R. M., Rohatgi, P. K., Sobczak, N., Sobczak, J., "Ferrous Composites: A review", Proceedings of the 29th Conference of High Temperature Capillarity, Poland, 1997.
2. Jing, W., Yisan, W., Yichao, D., "Production of (Ti,V)C reinforced Fe matrix composite, Materials Science and Engineering", A 454–455, 2007, 75–79.
3. Jing, W., Yisan, W., Yichao, D., Wei, G., "Microstructure and wear-resistance of Fe–(Ti,V)C composite", Materials and Design, 28, 2007, 2207–2209.
4. Das, K., Bandyopadhyay, T. K., Das, S., "A Review on the various synthesis routes of TiC reinforced ferrous based composites", Materials science, 37, 2002, 3881 – 3892.
5. Pagounis, E., Talvitie, M., Lindross, V. K., "Influence of reinforcement volume fraction and size on the microstructure and abrasion wear resistance of hot isostatic pressed white iron matrix composite", Metallurgical and Materials Transactions, A 27, 1997, 4171–4181.
6. Wang, Y., Zhang, X., Zeng, G., Li, F., "Cast sinter technique for producing iron base surface composites", Materials and Design, 21, 2000, 447-452
7. Razavi, M., Rahimipour, M. R., "Effect of mechanical activation on syntheses temperature of TiC reinforced iron-based nano-composite from ilmenite concentrate", Ceramics International, 35, 2009, 3529–3532.
8. Razavi, M., Rahimipour, M. R., Rajabi-Zamani, A. H., "Effect of nanocrystallineTiC powder addition on the hardness and wear resistance of cast iron", Materials Science and Engineering, A 454–455, 2007, 144–147.
9. Jayasankar, K., Mandal, A., Pany, A., Mukherjee, P. S., "Synthesis of Fe-TiC in-situ composites by plasma smelting of ilmenite", Materials and Manufacturing Processes, 26, 2011, 1330–1334.
10. Kennedy, A. R., Karantzalis, A. E., Wyatt, S. M., "The microstructure and mechanical properties of TiC and TiB_2-reinforced cast metal matrix composites", Journal of Materials Science, 34, 1999, 933– 940.
11. Li, B., Liu, Y., Cao, H., He, L., Li, J., "Rapid fabrication of in situ TiC particulates reinforced Fe-based composites by spark plasma sintering", Materials Letters, 63, 2009, 2010–2012.
12. Saidi, A., Chrysanthou, A., Wood, J. V., Kellie, J. L. F., "Characteristics of the combustion synthesis of TiC and Fe–TiC composites", Journal of Materials Science, 29, 1994, 4493–4998.
13. Terry, B. S., Chinyamakobvu, O. S., "In situ production of Fe-TiC composites by reactions in liquid iron alloys", Journal of Materials Science Letters, 10, 1991, 628-629.
14. Razavi, M., Yaghmaee, M. S., Rahimipour, M. R., Razavi Tousi, S. S., "The effect of production method on properties of Fe–TiC composite", International Journal of Mineral Processing, 94, 2010, 97-100.
15. Dogan, O. N., Hawk, J. A., "In-mold method for casting in situ Fe-TiC composites", Microstructural Science, 23, 1996, 251.
16. Licheri, R., Orru, R., Cao, G., Crippa, A.,

[DOI: 10.22068/ijmse.12.2.56]

Scholz, R., "Self-propagating combustion synthesis and plasma spraying deposition of TiC–Fe powders", Ceramics International, 29, 2003, 519–526.
17. Persson Anders, P., Jarfors, E. W., Savage, S., "Self-propagating high-temperature synthesis and liquid-phase sintering of TiC/Fe composites", Journal of Materials Processing Technology, 127, 2002, 131–139.
18. Capaldi, M. J., Saidi, A., Wood, J. V., "Reaction synthesis of TiC and Fe-TiCcomposites", ISIJ International, 37, 1997, 188-193.
19. Jing, W., Yisan, W., "In-situ production of Fe–TiC composite", Materials Letters, 61, 2007, 4393–4395.
20. Galgali, R. K., PhD thesis, Indian Institute of Technology, Kharagpur, 1995.
21. Terry, B. S., Chinyamakobvu, O. S., "Material Science and Technology", 7, 1991, 842.
22. Bandyopadhyay, T. K., Chatterjee, S., Das, K., "Synthesis and characterization of TiC-reinforced iron-based composites", Part I On synthesis and microstructural characterization, Journal of Materials Science, 39, 2004, 5735 – 5742.
23. Tjong, S. C., Chen, H., "Nanocrystalline materials and coatings", Materials Science and Engineering, R 45, 2004, 1–88.
24. Suryanarayana, C., "Mechanical alloying and milling", Materials Science, 46, 2001, 1-184.
25. Balaz, P., "Mechanical activation in hydrometallurgy", Internatinal Journal of Mineral Processing, 72, 2003, 341– 354.
26. Kleiner, S., Bertocco1, F., Khalid, F. A., Beffort, O., "Decomposition of process control agent during mechanical millingand its influence on displacement reactions in the Al–TiO_2 system", Materials Chemistry and Physics, 89, 2005, 362–366.
27. Zhang, D. L., "Processing of advanced materials using high-energy mechanical milling", Progress in Materials Science, 49, 2004, 537–560.
28. Razavi, M., Rahimipour, M. R., Ebadzadeh, T., Razavi Tousi, S. S., "Syntheses of Fe–TiC nanocomposite from ilmenite concentrate via microwave heating", Bulletin of Materials Science, 32, 2009, 155-160.
29. Raygan, S., Vahdati Khaki, J., Aboutalebi, M. R., "On the behaviourof hematite and graphite blend during ball milling and heating up reduction of milled mixture", Steel Research International, 75, 2004, 161-166.
30. Pourghahramani, P., Forssberg, E., "Effects of mechanical activation on the reduction behavior of hematite concentrate", Internatinal Journal of Mineral Processing, 82, 2007, 96–105.
31. Vahdatikhaki, J., Aboutalebi, M. R., Raygan, S., "The effect of mechanical milling on the carbothermic reduction of hematite, Mineral Processing and Extractive Metallurgy Review", 24, 2003, 1-19.
32. Kashiwaya, Y., Suzuki, H., Ishii, K., "Gas Evolution during Mechanical Milling of Hematite–Graphite Mixture", ISIJ International, 44, 2004, 1970–1974.
33. Setoudeh, N., Saidi, A., Welham, N. J., "Carbothermic reduction of anatase and rutile", Journal of Alloys and Compounds, 390, 2005, 138–143
34. Razavi, M., Rahimipour, M. R., Kaboli, R., "Synthesis of TiC nanocomposite powder from impure TiO_2 and carbon black by mechanically activated sintering", Journal of Alloys and Compounds, 460, 2008, 694–698.
35. Das, K., Bandyopadhyay, T. K., "Effect of form of carbon on the microstructure of in situ synthesized TiC-reinforced iron-based composite", Materials Letters, 58, 2004, 1877–1880.
36. Yang, Y. F., Wang, H. Y., Liang, Y. H., Zhao, R. Y., Jiang, Q. C., "Effect of C particle size on the porous formation of TiC particulate locally reinforced steel matrix composites via the SHS reaction of Ni–Ti–C system during casting", Materials Science and Engineering, A 474 , 2008, 355–362.
37. Wang, Y., Zhang, X., Li, F., Zeng, G., "Study on an Fe-TiC surface composite produced in situ", Materials and Design, 20, 1999, 233–236
38. Welhamand, N. J., Wiliams, J. S., "Carbothermic reduction of ilmenite and rutile", Metallurgical and Materials Transactions B, 30, 1999, 1075–1081.
39. Fengjun, C., Yisan, W., "Microstructure of Fe-TiCsurface composite poduced by cast-sintering", Materials Letters, 61, 2007, 1517–1521.

[DOI: 10.22068/ijmse.12.2.56]

40. Takacs, L., "Self-sustaining reactions induced by ball milling", Progress in Materials Science, 47, 2002, 355–414.
41. Cullity, B. D., "Elements of X-ray Diffraction", Addison-Wesly, Reading, MA, 1978.
42. Williamson, G. K., Hall, W. H., "X-ray line broadening from filed aluminum and wolfram", ActaMetalurgical, 1, 1953, 21-31.
43. Liu, Z. G., Lu, L., Lai, M. O., "Synthesis of nanocrystalline carbide in tungsten alloy by mechanical alloying and annealing", Journal of Alloys and Compounds, 394, 2005, 176–180.
44. Properties and characteristics of graphite for the semiconductor industry, 2013.
45. Terzic, R. K., "Microstructure and physical-chemical properties of petroleum coke as carburizer", NAFTA, 61, 2010, 136-139.
46. Milenkova, K. S., Borrego, A. G., Alvare, D., Xiberta, J., Menendez, R., "Devolatilisation behaviour of petroleum coke under pulverized fuel combustion conditions", Fuel, 82, 2003, 1883–1891.
47. Kashiwaya, Y., Ishii, K., "Analysis of the transition state of the carbon and iron oxide mixture activated by mechanical milling", ISIJ International, 44, 2004, 1981-1990.
48. Kashiwaya, Y., Suzuki, H., Ishii, K., "Characteristics of nano-reactor and phenomena during mechanical milling of hematite–graphite mixture", ISIJ International, 44, 2004, 1975-1980.
49. Swift, G. A., Koc, R., "Formation studies of TiC from carbon coated TiO_2", Journal of Materials Science,34, 1999, 3083 – 3093
50. Lee, G. G., Kim, B. K., "Effect of raw material characteristics on the carbothermalreduction of titanium oxide", Materials Transactions, 44, 2003, 2145-2150.
51. Lee, P. Y., Koch, C. C., "Formation of amorphous Ni-Zr alloy powder by mechanical alloying of intermetallic powder mixtures and mixtures of nickel or zirconium with intermetallics", Journal of Materials Science, 23, 1988, 2837-2845.

[DOI: 10.22068/ijmse.12.2.56]